Research on moving load identification based on measured acceleration and strain signals

Yun Zhou

Key Laboratory for Damage Diagnosis of
Engineering Structures of Hunan Province,
Hunan University,
Changsha, Hunan, 410082, China
and
College of Civil Engineering,
Hunan University,
Changsha, Hunan, 410082, China
Email: zhouyun05@gmail.com

Sai Zhou

Key Laboratory of Building Safety and Energy
Efficiency of the Ministry of Education,
College of Civil Engineering,
Hunan University,
Changsha, Hunan, 410082, China
Email: zhousai2017@163.com

Lu Deng*

Key Laboratory for Damage Diagnosis of
Engineering Structures of Hunan Province,
Hunan University,
Changsha, Hunan,
410082, China
Email: denglu@hnu.edu.cn
*Corresponding author

Songbai Chen

Hunan Provincial Key Laboratory of Green Advanced Civil,
Engineering Materials and Application Technology,
College of Civil Engineering,
Hunan University,
Changsha, Hunan, 410082, China
Email: 543880539 @qq.com

Weijian Yi

College of Civil Engineering,
Hunan University,
Changsha, Hunan, 410082, China
Email: hunuyi2006@gmail.com

Abstract: Moving load identification from the dynamic responses of bridges is a typical inverse problem that is solved to estimate vehicle axle loads in motion from observed data. To reduce the ill-posedness of the problem and improve solution accuracy, this paper proposes a method for reconstructing the dynamic displacement response via combining the measured acceleration and strain signals for moving load identification. The identification accuracy achieved by employing the reconstructed displacement under different vehicle speeds and different identification algorithms was investigated via finite element (FE) analysis, and a laboratory experiment of a simply supported beam model was constructed to validate the effectiveness of the proposed method. Both the computation simulations and experimental results indicate that the reconstructed displacements fit the true values well and the proposed method can effectively overcome the ill-posedness of the problem in terms of equation resolution and achieve a high level of accuracy.

Keywords: moving load identification; acceleration; dynamic strain; signal reconstruction; modal decomposition.

Reference to this paper should be made as follows: Zhou, Y., Zhou, S., Deng, L., Chen, S. and Yi, W. (2019) 'Research on moving load identification based on measured acceleration and strain signals', *Int. J. Lifecycle Performance Engineering*, Vol. 3, Nos. 3/4, pp.257–288.

Biographical notes: Yun Zhou received his PhD in Civil Engineering from Hunan University in 2008. He is a Professor in the College of Civil Engineering at Hunan University. His research interests include structural health monitoring and structural identification.

Sai Zhou is a graduate student in Civil Engineering at Hunan University. Her research interest lies in moving load identification of bridges.

Lu Deng received his PhD in Civil Engineering from Louisiana State University in 2009. He is a Professor in the College of Civil Engineering at Hunan University. His research interests include vehicle-bridge coupled vibration and condition assessment of bridges.

Songbai Chen is a Master student majoring in Civil Engineering at Hunan University. His research interests include moving load identification and dynamic signal processing.

Weijian Yi received his PhD in Civil Engineering from Hunan University in 1989. He is a Professor in the College of Civil Engineering at Hunan University. His research interests include the basic theories of reinforced concrete structures and seismic design of reinforced concrete structures.

1 Introduction

The amplitude of moving vehicle loads on bridges has a considerable influence on their service life. Moreover, dramatically increasing traffic volumes and overweight trucks may cause fatigue and serious damage to a bridge structure, even leading to bridge collapse in some extreme cases (Beizma and Schanack, 2007; Lydon et al., 2016; Wang et al., 2016). Therefore, vehicle loads in motion must be identified by employing advanced and reliable techniques for bridge design and maintenance.

Extensive studies on moving load identification have been conducted by scholars in the last 30 years. Most of these studies simplified the bridge as a uniform simply supported beam or multi-span continuous beam. O'Connor and Chan (1988) proposed interpretive method I (IMI) using on-site measurements of bridge strains for dynamic wheel load identification. Law et al. (1997) proposed a time domain method (TDM) based on modal superposition theory to identify the dynamic interaction forces in the time domain by using bending moment and acceleration measurements simultaneously. Law et al. (1999) used a new method, the frequency-time domain method (FTDM), to acquire the time histories of moving forces by converting a set of equations relating the Fourier transform into the time domain. Both the TDM and FTDM are based on system identification theory. The interpretive method II (IMII), introduced by Chan et al. (1999), identifies the time-varying moving loads by numerical methods based on Euler's beam theory instead of the beam element model, which differs from IMI. Thereafter, quite a few comparative studies (Chan et al., 2000, 2001a, 2001b; Yu and Chan, 2007; Zhu and Law, 2002b) were conducted to investigate the influence of various parameters on the four classic methods (IMI, IMII, TDM and FTDM) applied for moving force identification system (MFIS). In addition to the system identification technique, the finite element (FE) method was used for the dynamic axle load identification research based on the vehicle-bridge coupled system (Law et al., 2004; Deng and Cai, 2010b, 2011; Zhu and Law, 2003b). To improve the accuracy in solving over determined set of equations, the singular value decomposition (SVD) technique (Yu and Chan, 2002, 2003, 2007) and the truncated generalised SVD algorithm (Chen and Chan, 2017) were employed to identify the force history. Since the nature of the inverse problem is ill-conditioned (Sanchez and Benaroya, 2014; Yu et al., 2016; O'Brien et al., 2008), regularisation, especially Tikhonov regularisation, is often utilised to provide bounds to the ill-conditioned forces and effectively reduce the noise corruption (Law and Zhu, 2000; Zhu and Law, 2002a; Law et al., 2001; Law and Fang, 2001; Zhu and Law, 2006; González et al., 2008). The updated static component (USC) technique has also been adopted in several studies (Asnachinda et al., 2008; Pinkaew, 2006; Pinkaew and Asnachinda, 2007) to eliminate the difficulty of an optimal regularisation selection and achieve a higher efficiency. Besides, the modified preconditioned conjugate gradient (M-PCG) method (Chen et al., 2018) was proved more robust to ill-conditioned equations in dealing with inverse problems, and the optimisation algorithm was available in moving load estimation (Pan and Yu, 2014). In the field of MFIS for the continuous bridges, a series of studies have been carried out and achieved good accuracy (Chan and Ashebo, 2006; Chan et al., 2006; Zhu and Law, 1999, 2001b, 2006). The multiple vehicle axle loads on a multi-span continuous bridge were successfully identified based on the least squares regularisation optimisation (Asnachinda et al., 2008). In terms of expanded applications, a case that a vehicle travelling on slab-type bridges was also discussed (Zhu

and Law, 2001a, 2003a, 2003b, 2003c; Law et al., 2007), in which the bridge deck was modelled as an orthotropic plate and the moving loads were estimated from the dynamic responses. The measured time-domain responses can also be employed to identify the pre-stressed force of a pre-stressed concrete bridge by a system identification approach (Chan and Yung, 2000; Law and Lu, 2005; Lu and Law, 2005). In addition, numerous achievements in moving load identification have been made in recent years with the application of artificial neural networks (ANNs) (Lu et al., 1993; Park et al., 2009; Kowm et al., 2014) and genetic algorithms (GAs) (Deng and Cai, 2010a).

Based on previous studies, two fundamental problems exist in moving load identification:

1 The measured response may not be a part of the true response data collection induced by load excitations, which may result in non-solution to the motion equations.

2 Tiny measurement errors in signals may lead to critical mistakes, which are biases of the solution due to the ill-conditioned matrix; therefore, the emphasis of solving the inverse problem lies in how to solve the ill-posed equations, and to correctly estimate the time history of the moving loads, the dynamic algorithms must be optimised and improved and the measurement errors must be eliminated.

In the dynamic inspection of a bridge, acceleration and dynamic strain are generally measured along the bridge, thus efficiently utilising both of these two kinds of data are desired to improve the identification accuracy. In this paper, a novel moving load identification method is proposed by utilising measured acceleration and strain signals on a bridge. The dynamic displacement of a bridge subjected to moving loads consists of the vibration displacement caused by inertia force as well as the static displacement caused by static force. The acceleration and strain signals were measured simultaneously to improve the identification accuracy. The dynamic displacement was reconstructed by a series of signal processing processes, including decomposition, optimisation and conversion of the strain and acceleration signals. The reconstructed vibration displacement signal was obtained by the integration of measured acceleration, and the static displacement signal was deduced from the measured strain signals utilising the curvature function fitted with the least mean squares method. Finally, the reconstructed dynamic displacement was used to identify the moving loads after superposition of vibration and static displacements. To verify the accuracy of the proposed method, a simply supported girder bridge with a span length of 25 m was set up by numerical simulation, and a set of dual-axle time-varying loads was applied to the bridge. Then, the IMII and TDM algorithms were used to evaluate the accuracy and reliability of the identified loads. The tested model for vehicle load identification was further constructed in the laboratory to verify the feasibility of the proposed method in an experiment, and the moving loads under different weights and speeds cases were successfully identified by the reconstructed displacement.

2 Reconstruction of dynamic displacement

The dynamic displacement of a beam under the moving loads is composed of not only the vibration displacement caused by inertial force but also the static displacement caused by

static loads. To obtain acceptable results, a signal processing scheme was applied to the directly measured data, and the dynamic displacement was reconstructed based on the strain and acceleration signals, as shown in Figure 1.

Figure 1 Reconstruction of dynamic displacement signal

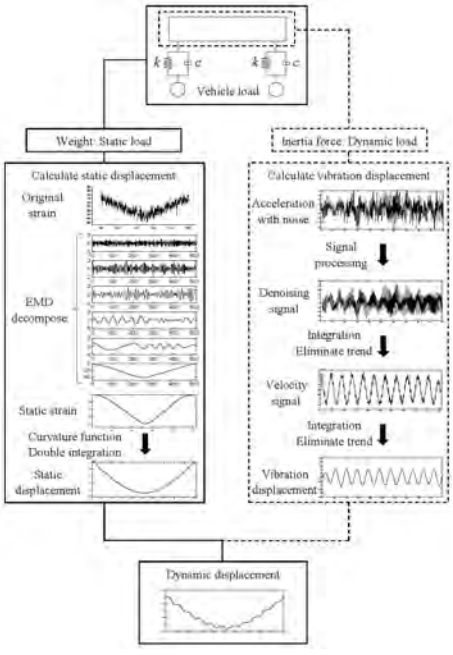

3 Theory of moving load identification

3.1 Equilibrium equation of vibration

The bridge can be simplified as a simply supported beam model to demonstrate the method. The beam is assumed to have a constant cross-section with a span length L, constant mass per unit length ρ, constant flexural stiffness EI and viscous proportional damping ratio C. The beam is assumed to be a Euler-Bernoulli beam without consideration of shear deformation and rotary inertia. When the time-varying point force $P(t)$ is moving on the beam from left to right at a speed of c, as shown in Figure 2, the vibration equation of the beam can be expressed as shown in equation (1).

$$\rho \frac{\partial^2 (x,t)}{\partial t^2} + C \frac{\partial v(x,t)}{\partial t} + EI \frac{\partial^4 v(x,t)}{\partial x^4} = \delta(x - ct) P(t) \tag{1}$$

where $v(x, t)$ is the deflection at point x and time t and $\delta(x - ct)$ is the Dirac delta function.

Figure 2 Simply supported beam for moving load identification

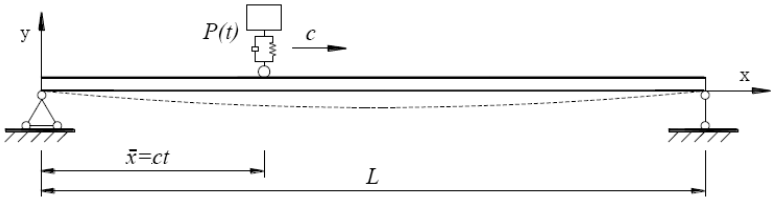

The n^{th} mode shape function of the beam can be written as $\phi_n(x) = \sin(n\pi x/L)$. Hence, the solution of equation (1) can be assumed to follow the form of equation (2):

$$v(x, t) = \sum_{n=1}^{\infty} \phi_n(x) q_n(t) \tag{2}$$

where n is the mode number and $q_n(t)$ (n = 1, 2, 3, …, ∞) are the displacements of the nth mode. By substituting equation (2) into equation (1), integrating the resultant equation with respect to x between 0 and l, and introducing the boundary conditions of the simply supported beam, the equation of motion (EOM) can be expressed in generalised modal coordinates, as shown in equation (3):

$$\ddot{q}_n(t) + 2\xi_n \omega_n \dot{q}_n(t) + \omega_n^2 q_n(t) = \frac{2}{\rho L} P_n(t) \quad (n = 1, 2, 3, \ldots, \infty) \tag{3}$$

where $\omega_n = \frac{n^2\pi^2}{L^2}\sqrt{\frac{EI}{\rho}}$, $\xi_n = \frac{C}{2\rho\omega_n}$ and $P_n(t) = P(t)\sin\left(\frac{n\pi\bar{x}}{L}\right)$ indicate the modal frequency, modal damping and modal force of the nth mode, respectively. $\bar{x}$ is the distance from the concentrated force to the left side support. If the time-varying force $P(t)$ is known, the modal displacements $q_n(t)$ can be obtained from equation (3); thus, the dynamic deflection $v(x, t)$ can be calculated by equation (2). The calculation process is a typical forward problem. The unknown load $P(t)$ can be deduced by acquiring the displacement, velocity and acceleration data at each measurement point of the structure.

3.2 Interpretive method II

When the boundary conditions correspond to the simply supported case, the exact solution for the bridge responses under dynamic forces can be deduced (Chan et al., 1999). If n moving loads are applied to the beam, using the modal decomposition method, equation (3) can be written as

$$\begin{Bmatrix} \ddot{q}_1(t) \\ \ddot{q}_2(t) \\ \vdots \\ \ddot{q}_n(t) \end{Bmatrix} + \begin{Bmatrix} 2\xi_1\omega_1\dot{q}_1(t) \\ 2\xi_2\omega_2\dot{q}_2(t) \\ \vdots \\ 2\xi_n\omega_n\dot{q}_n(t) \end{Bmatrix} + \begin{Bmatrix} \omega_1^2 q_1(t) \\ \omega_2^2 q_2(t) \\ \vdots \\ \omega_n^2 q_n(t) \end{Bmatrix} =$$

$$\frac{1}{\rho L}\begin{bmatrix} \sin\dfrac{\pi(ct-\hat{x}_1)}{L} & \sin\dfrac{\pi(ct-\hat{x}_2)}{L} & \cdots & \sin\dfrac{\pi(ct-\hat{x}_k)}{L} \\ \sin\dfrac{2\pi(ct-\hat{x}_1)}{L} & \sin\dfrac{2\pi(ct-\hat{x}_2)}{L} & \cdots & \sin\dfrac{2\pi(ct-\hat{x}_k)}{L} \\ \vdots & \vdots & \vdots & \vdots \\ \sin\dfrac{n\pi(ct-\hat{x}_1)}{L} & \sin\dfrac{n\pi(ct-\hat{x}_2)}{L} & \cdots & \sin\dfrac{n\pi(ct-\hat{x}_k)}{L} \end{bmatrix} \begin{Bmatrix} P_1(t) \\ P_2(t) \\ \vdots \\ P_k(t) \end{Bmatrix} \tag{4}$$

where $\hat{x}_k$ is the distance from the k^{th} load to the first load and $\hat{x}_1 = 0$ when $k = 1$.

If P_1, P_2, …, P_k are constant moving loads when ignoring the effect of damping, equation (1) has the following closed-form solution:

$$v(x,t) = \frac{L^3}{48EI}\sum_{i=1}^{k} P_i(x)\sum_{n=1}^{\infty}\frac{1}{n^2(n^2-\alpha^2)}\sin\frac{n\pi x}{L}\left[\sin\frac{n\pi(ct-\hat{x}_i)}{L} - \frac{\alpha}{n}\sin\omega_n\left(t-\frac{\hat{x}_i}{c}\right)\right] \tag{5}$$

where $\alpha = \dfrac{\pi v}{L\omega_n}$. As long as the displacements at x_1, x_2, …, x_n are available, the magnitude of each constant moving load can be acquired from equation (6):

$$\{v\} = [S_{vp}]\{P\} \tag{6}$$

where $[S_{vp}] = \begin{bmatrix} S_{11} & \cdots & S_{1i} & \cdots & S_{1k} \\ \vdots & \ddots & & & \vdots \\ S_{m1} & & S_{mi} & & S_{mk} \\ \vdots & & & \ddots & \vdots \\ S_{l1} & \cdots & S_{li} & \cdots & S_{lk} \end{bmatrix}$ and $S_{mi} = \dfrac{L^3}{48EI}\sum_{n=1}^{\infty}\dfrac{1}{n^2(n^2-\alpha^2)}\sin\dfrac{n\pi x}{L}\left(\sin\dfrac{n\pi(ct-\hat{x}_i)}{L} - \dfrac{\alpha}{n}\sin\omega_n\left(t-\dfrac{\hat{x}_i}{c}\right)\right)$

where l and k indicate the number of displacement measurement stations and axle loads, respectively. If $l \geq k$, the load can be estimated by the least squares method, as shown in equation (7).

$$P\left([S_{vp}]^T[S_{vp}]\right)^{(-1)}[S_{vp}]^T\{v\} \tag{7}$$

Accordingly, this method can be applied to estimate moving time-varying axle loads from equation (4), in which the values of the axle loads at any time can be solved using the least squares method.

3.3 Time domain method

The TDM uses modal superposition to identify time-varying axle loads in the time domain. Based on the motion equation, the modal displacement $q_n(t)$ can be solved from equation (3) via a convolution integral in the time domain (Law et al., 1997).

$$q_n(t) = \frac{1}{M_n}\int_0^t h_n(t-\tau)P_n(t)d\tau \tag{8}$$

where $h_n(t) = \frac{1}{\omega_n'} e^{-\xi_n\omega_n t}\sin(\omega_n' t)(t \geq 0)$, in which $\omega_n' = \omega_n\sqrt{1-\xi_n^2}$, $M_n = \frac{2}{\rho L}$.

When substituting equation (8) into equation (2), the dynamic deflection of the beam at point x and time t can be expressed as follows:

$$v(x,t) = \sum_{i=1}^{\infty}\frac{1}{M_n\omega_n'}\sin\frac{n\pi x}{L}\int_0^t e^{-\xi_n\omega_n(t-\tau)}\sin\omega_n'(t-\tau)\sin\frac{n\pi c\tau}{L}P(\tau)d\tau \tag{9}$$

The bending moment of the beam at point x and time t can be expressed as shown in equation (10).

$$\begin{aligned} M(x,t) &= -EI\frac{\partial^2 v(x,t)}{\partial x^2} \\ &= \sum_{n=1}^{\infty}\frac{2EI\pi^2 n^2}{\rho L^3\omega_n'}\sin\frac{n\pi x}{L}\int_0^t e^{-\xi_n\omega_n(t-\tau)}\sin\omega_n'(t-\tau)\sin\frac{n\pi c\tau}{L}P(\tau)dt \end{aligned} \tag{10}$$

Assuming that the time-varying load $P(t)$ is a step function in a short time interval Δt, equation (10) can be rewritten in discrete terms as

$$\begin{aligned} &M(i) = \frac{2EI\pi^2}{\rho L^3}\sum_{n=1}^{\infty}\frac{n^2}{\omega_n'}\sin\frac{n\pi x}{L}\sum_{j=0}^{i}e^{-\xi_n\omega_n\Delta t(i-j)}\sin\omega_n'\Delta t(i-j)\sin\frac{n\pi c\Delta tj}{L}P(j)\Delta t, \\ &i = 0, 1, 2, 3, \ldots, N \end{aligned} \tag{11}$$

where Δt is the sampling time interval and $N + 1$ is the number of sample points.

When a vehicle enters onto and leaves the bridge, assuming that $P(0) = P(N_E) = 0$ such that $M(0) = M(1) = 0$, then equation (11) can be rewritten in the matrix form as shown in equation (12).

$$\begin{Bmatrix} M(2) \\ M(3) \\ \vdots \\ M(N) \end{Bmatrix} = \sum_{i=1}^{\infty} C_{xn} \times \begin{bmatrix} E_n^1 S_1(1)S_2(1) & 0 & \ldots & 0 \\ E_n^2 S_1(2)S_2(1) & E_n^1 S_1(1)S_2(2) & \ldots & 0 \\ \vdots & \vdots & \vdots & \vdots \\ E_n^{N-1} S_1(N-1)S_2(1) & E_n^{N-2} S_1(N-2)S_2(2) & \ldots & b_{ee} \end{bmatrix} \times \begin{Bmatrix} P(1) \\ P(2) \\ \vdots \\ P(N_B - 1) \end{Bmatrix} \tag{12}$$

Where $C_{xn} = \frac{2EI\pi^2}{\rho L^3}\frac{n^2}{\omega_n'}\sin\frac{n\pi x}{L}\Delta t$, $E_n^{i-j} = e^{-\xi_n\omega_n\Delta t(i-j)}$, $S_1(i-j) = \sin\omega_n'\Delta t(i-j)$, and $S_2(j) = \sin\left(\frac{n\pi c\Delta t}{L}j\right)$. $M(i)$ is the bending moment of the i^{th} time step, $P(i)$ is the axle load at the i^{th} time step, the subscript N denotes the number of sampling points for the measured bending moment response, $N_B = L/c\Delta t$ indicates the number of sampling points for the time-varying load moving through the entire bridge deck, and

$$b_{ee} = E_n^{N-N_B+1}S_1(N-N_B+1)S_2(N_B-1) \tag{13}$$

Equation (12) can be simplified as

$$[B]\{P\} = \{M\} \tag{14}$$

where $[B]$ is a coefficients matrix relating the parameters of the vehicle-bridge system; $\{P\}$ is the time-varying load vector; and $\{M\}$ is the vector of the bending moment responses. If $N = N_B$ and $[B]$ is a lower triangular matrix, the load vector $\{P\}$ can be directly solved by equation (14). If $N > N_B$ or there are N_l responses for the bending moment ($N_l > 1$) from the measuring points, $\{P\}$ can be obtained by the least squares method. In addition, equation (14) can be utilised to perform load identification referring to a two-axle vehicle load based on the linear superposition principle.

The above procedure is derived for single force identification. Equation (14) can be modified for two-force identification using the linear superposition principle (Law et al., 1997)

$$\begin{bmatrix} B_a & 0 \\ B_b & B_a \\ B_c & B_b \end{bmatrix}\begin{Bmatrix} P_1 \\ P_2 \end{Bmatrix} = \{M\}, \tag{15}$$

where B_a $[N_s \times (N_B - 1)]$, B_b $[(N - 1 - 2N_s) \times (N_B - 1)]$ and B_c $[N_s \times (N_B - 1)]$ are submatrices of matrix B. The first row of submatrices in the first matrix describes the state of having the first force on the beam after its entry. The second and third rows of submatrices describe the states having two forces on the beam and one force on the beam after the exit of the first force. The entire matrix has dimensions of $(N - 1) \times (N_B - 1)$. $N_s = l_s/c\Delta t$, where l_s is the distance between the two forces. The two forces can be identified using more than one bending moment measurement.

4 Displacement caused by the static load

The static displacement is obtained through the strain signal caused by the static load. After performing empirical mode decomposition (EMD) on the strain signal, the high-frequency component will be filtered to extract the time history curve of the static strain. Then, the curvature function of the beam can be obtained by the least squares method. Finally, the vertical displacement involved with the static load is estimated by the relationship between the curvature and vertical displacement.

4.1 Empirical mode decomposition

The Hilbert-Huang transform (HHT) method is proposed for non-stationary and nonlinear signal analysis by Huang (2000). The key step of HHT is to use the EMD method that decomposes the complex signal into a collection of intrinsic mode functions (IMFs). Since the decomposition is based on the local characteristic time scale of the data, mean or zero reference is not required in the EMD method, which is adaptive and efficient for analysing non-stationary and nonlinear time series.

The EMD method is based on the following assumptions (Huang et al., 1998):

1 The signal has at least two extremes, one maximum and one minimum.

2 The local characteristic time scale is defined by the time lapse between the extrema.

3 If the data were totally devoid of extrema but contained only inflection points, then they can be differentiated once or more times to reveal the extrema. The final results can be obtained by integrating the components.

Each IMF extracted by the sifting process satisfies two conditions:

1 the number of extrema and the number of zero crossings must either equal or differ at most by one

2 the envelope is defined by the local minima.

An IMF involves only one mode of oscillation embedded in the vibration signal and gives rise to a well-defined instantaneous frequency. By using the EMD method, the original multicomponent signal is decomposed into a series of mono-components, making it accessible for further analysis, while some problems remain in the decomposed result, such as end effects and the mode mixing problem.

4.2 Displacement by the curvature function

For the beam, the displacement v is defined as the deflection of the cross-section in the direction perpendicular to the neutral axis during bending deformation. The neutral axis forms a plane curve in the central principle plane of inertia, which is called the deflection curve. The strain ε represents the deformation of the infinitesimal element per unit length subjected to stress, and the curvature k indicates the bending extent of the beam. An element with length dx is randomly selected from the bending beam, as shown in Figure 3, where O_1O_2 is the neutral axis of the beam element; y is the distance from the edge to the neutral axis; ρ is the radius of curvature; and the length of the neutral axis remains constant before and after the deformation.

Thus, the length change Δs of the beam edge can be expressed as

$$\Delta s = l_{ab} - l_{O_1O_2} = (\rho + y)d\theta - \rho d\theta = yd\theta \tag{16}$$

Accordingly, the magnitude of strain ε can be calculated as

$$\varepsilon = \frac{\Delta s}{dx} = \frac{yd\theta}{\rho d\theta} = \frac{y}{\rho} \tag{17}$$

In equation (17), the strain and curvature at the same location are linearly correlated. According to the differential theorem and ignoring the effect of second-order terms, the deflection-curvature relationship can be expressed as

$$\frac{1}{\rho(x)} = \frac{d^2v}{d^2x} \tag{18}$$

The deflection curve can be obtained by integrating the beam curvature function twice, and the strain and curvature at the same cross-section are linearly correlated; thus, the strain-deflection relationship can be formed through the curvature.

Figure 3 Curvature deformation of the beam element

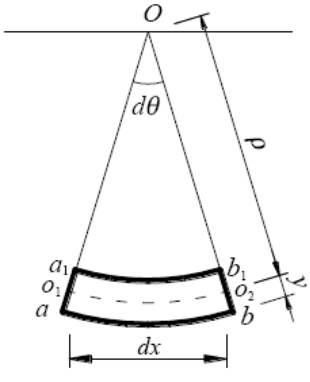

5 Displacement caused by the inertia force

Vibration displacement can be obtained by integrating the measured acceleration signal twice in the frequency domain. As shown in Figure 1, in the signal processing procedure, the signal should be filtered and the trend term should be eliminated before each step of integration, so the adaptive least-mean-square (LMS) algorithm for noise reduction is adopted.

5.1 LMS adaptive noise reduction

On the basis of the Wiener filter, the LMS algorithm developed with the minimum mean square error (MMSE) and the steepest-descent algorithm, which simulates a desired signal by finding the filter weights, is related to producing the least mean square of the error signal. Based on the gradient decent algorithm, the adaptive LMS filter updates the weights to approach the optimum values for minimising the error criterion.

Figure 4 Flowchart of LMS adaptive noise reduction

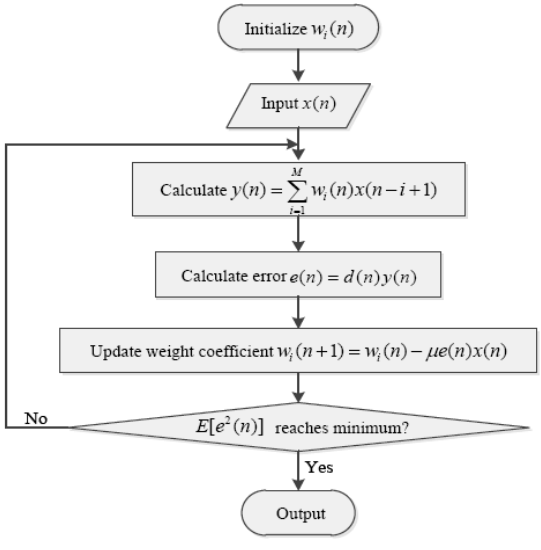

The main procedure of the adaptive LMS algorithm (Zhu et al., 2016) is as follows:

1 Calculate the output signal $y(n)$ from the adaptive filter:

$$y(n) = X^T(n)W(n) \tag{19}$$

where n indicates the number of iterations of the algorithm, $X(n)$ is the input signal in vector form and $W(n)$ is the filter weights in vector form.

2 By calculating the difference between the reference signal $d(n)$ and the filter's output $y(n)$, the error signal $e(n)$ is acquired as follows:

$$e(n) = d(n) - y(n) \tag{20}$$

3 Update the filter weights by the steepest-descent algorithm:

$$W(n+1) = W(n) + 2\mu e(n)X(n) \tag{21}$$

where $W(n + 1)$ indicates the filter weights for the next iteration and μ is the convergence factor, which can be used to control the filtering rate.

4 Repeat steps 1 to 3 until the algorithm converges, continuous iteration and updating the filter weights will contribute to achieving the minimum mean square error $E[e^2(n)]$. Meanwhile, the output signal $y(n)$ approaches the reference signal $d(n)$.

The LMS filter carries out filtering using only the observable signals $x(n)$, $d(n)$ and $e(n)$ without involving any matrix operations, so it has low computational complexity for

adaptive noise reduction. The flowchart of adaptive LMS algorithm for noise reduction is shown in Figure 4.

5.2 Integration in the frequency domain

Fourier transform can be performed to convert the signals from the time domain to the frequency domain. Meanwhile, the signal can be restored to the time domain by inverse Fourier transformation. Then, the displacement value in the time domain can be obtained from the signal by reserving its real part. The integration method is shown in the flowchart in Figure 5.

Figure 5 Flowchart of the integration method

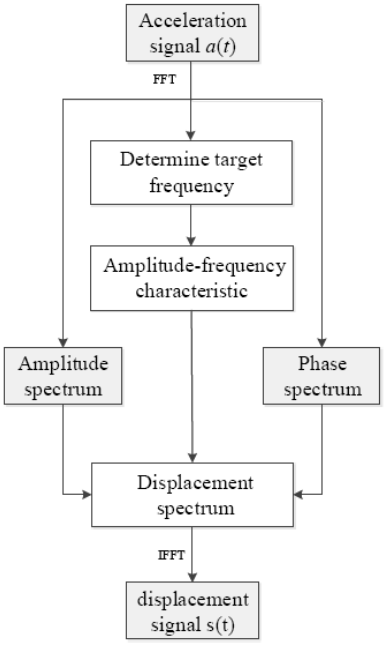

Assuming a discrete acceleration sequence $a(n)$ in the time domain with a data length N, the discrete Fourier transform (DFT) is performed according to equation (22).

$$\begin{cases} a(k) = \dfrac{1}{N}\sum_{1}^{N} a(n) e^{\left[\frac{-2\pi(k-1)(n-1)i}{N}\right]} = a_k + b_k i \\ f(k) = \dfrac{(n-1) f_0}{2N} \qquad (1 \le k \le N) \end{cases} \tag{22}$$

where $a(k)$ is the Fourier transform of the acceleration sequence $a(n)$, $f(k)$ is the corresponding frequency and f_0 is the sampling frequency. The amplitude A_k of the simple harmonics, the modal frequency ω_k and the initial phase ω_k, corresponding to $a(k)$, can be obtained by equation (23).

$$\begin{cases} A_k = \sqrt{a_k^2 + b_k^2} \\ \phi_k = \arctan\left(\dfrac{b_k}{a_k}\right) \\ \omega_k = 2\pi f_k \end{cases} \tag{23}$$

The simple harmonic wave is expressed as

$$a(t)_k = A_k \cos\left(\omega_k + \phi_k\right) \tag{24}$$

The displacement harmonic wave is available after double integration for $a(t)_k$, as shown in equation (25).

$$S(t)_k = A_{zk} \cos\left(\omega_{sk} t + \phi_{sk}\right) \tag{25}$$

where $A_{sk} = A_k / \omega_k^2$, $\phi_{sk} = \phi_k - \pi$, $\omega_{sk} = \omega_k$.

Based on the signal superposition principle, the displacement curve can be obtained as shown in equation (26).

$$S(t) = \sum_{k=1}^{N} S(t)_k = \sum_{k=1}^{N} A_{sk} \cos\left(\omega_{sk} t + \phi_{sk}\right) \tag{26}$$

By performing inverse Fourier transformation, the equation above can be rewritten as

$$F\left(s(t)\right) = H_s(\omega) F\left(\bar{a}(t)\right) = -\frac{1}{\omega^2} F\left(\bar{a}(t)\right) \Rightarrow s(t) = -F^{-1}\left[\frac{1}{\omega^2} F\left(\bar{a}(t)\right)\right] \tag{27}$$

where $F(x)$ indicates performing Fourier transform on the function, $H_e(\omega)$ is the transfer function, $a(t)$ is the acceleration signal in the time domain and $s(t)$ is the displacement signal obtained by integration.

Equation (27) shows that low-frequency noise contained in the acceleration signal will be amplified during the integration and cause a large error due to the amplitude-frequency characteristic $1/\omega^2$. Therefore, the integration error in calculating the displacement from the acceleration response can be constrained by filtering the low-frequency noise from the observed signals.

6 Numerical simulation

To validate the feasibility of the proposed method, a simply supported beam model was built in ANSYS for FE model analysis. The beam element was selected as BEAM3, where each element node had three degrees of freedom (DOFs). The following parameters were chosen for the modeled bridge: $EI = 2.87 \times 10^9$ N · m^2, ρ = 2,303 kg/m and L = 25 m. The beam was divided into 100 elements, and the first three natural

frequencies of the bridge were determined to be f_1 = 4.79 Hz, f_2 = 19.18 Hz and f_3 = 43.15 Hz by calculation. Assuming that dual-axle time-varying loads move on the bridge deck, the expressions of the load are as follows:

$$f_1(t) = -28.75\left(1 + 0.25\sin(2\pi t)\right) \tag{28}$$

$$f_2(t) = -57.5\left(1 + 0.25\sin(2\pi t)\right) \tag{29}$$

Three measuring points were assumed to be located at 1/4, 1/2, and 3/4 of the span along the beam. The acceleration and strain responses acquired from the measuring points were used for moving load identification, and the first three modes of the beam were of interest in the computation. The sampling frequency was set as 200 Hz to cover the first three modes as well as meet the requirement of the Nyquist-Shannon sampling theorem. Three load cases were designed and the moving load speeds were set as 10, 20, and 30 m/s.

In practical application and bridge tests, the magnitude of moving loads cannot be obtained by direct measurement. To assess the identified results, FE software is used to generate the true output signal from the measuring points, and then, the loads obtained from the true and reconstructed signals are compared for error evaluation using equation (30).

$$P_{error} = \frac{\sum \left| f_{ture} - f_{recon} \right|}{\sum \left| f_{ture} \right|} \times 100\% \tag{30}$$

where P_{error} represents the relative percentage error and f_{ture} and f_{recon} represent the loads identified from the true signal and reconstructed signal, respectively.

6.1 Static displacement identification

When the loads are moving across the bridge at a speed of 20 m/s, the dynamic responses of the three measuring points can be calculated directly from ANSYS, as shown in Figure 6.

When a car is travelling on the beam at a low speed, noises caused by the environment and instrument during data acquisition may corrupt the signals. To simulate the influence of environment noise, 10 dB of white noise was added to the strain generated from the FE software.

The dynamic strain signal was decomposed by the EMD method to acquire the corresponding IMFs at three points, one of which is illustrated in Figure 7, and the calculated static strains caused by the static loads at three points are respectively shown in Figure 8. As shown in the decomposed results, the EMD method decomposed the complex signal into multiple IMFs, where the low-frequency component IMF11 reflects the strain caused by static vehicle loads.

The neutral axis is at the middle height of each beam section, the curvature of multiple points can be derived from the nodal strain responses according to equation (17), and the curvature function of the entire beam is obtained by the least-squares method. Then, the deflection curve can be obtained by integrating the curvature function twice, as shown in equation (18). The static displacements at points 1, 2, and 3 subjected to static forces are shown in Figure 9.

Figure 6 Moving load response at the instrument for v = 20 m/s, (a) acceleration signals (b) dynamic displacement signals (c) dynamic moment signals

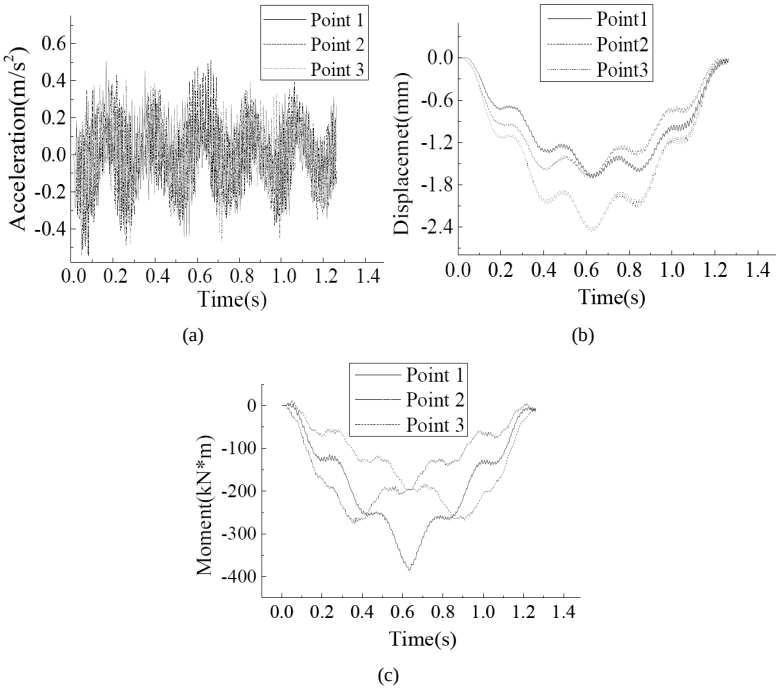

Figure 7 EMD decomposition of the strain signals at point 2

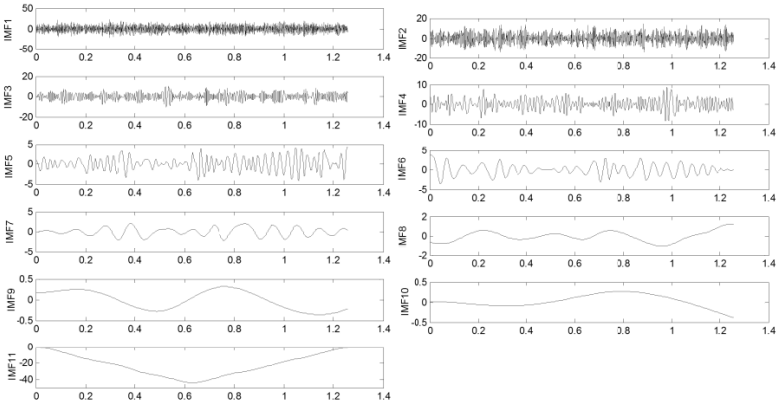

Figure 8 Strain signal decomposition, (a) at point 1 (b) at point 2 (c) at point 3

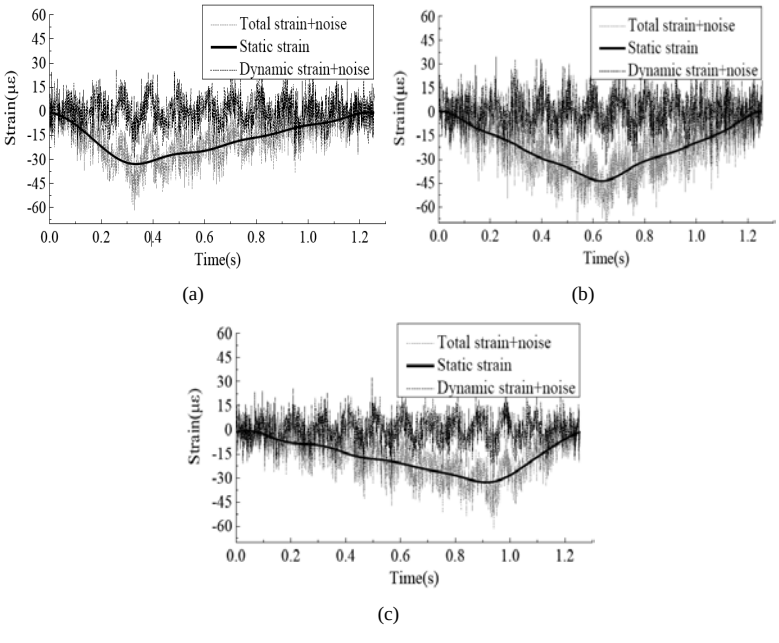

Figure 9 Identification results of displacement caused by static loads

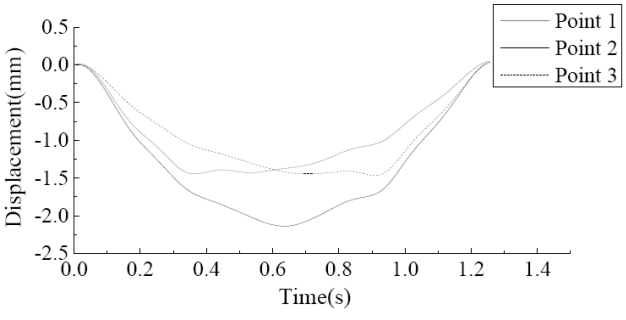

6.2 Vibration displacement identification

The true value and the value after adding 5 dB of white noise to the acceleration signals are shown in Figure 10. Since the signal after adding white noise contained many interference frequencies, the adaptive LMS algorithm was utilised to reduce the noise. The filter order was set as 100, and the step factor was set as 0.005. The frequency

domain characteristics of the filtered signal are shown in Figure 11, illustrating that the filtered signal is largely consistent with the true signal except for a small amount of noise mixed in the high-frequency components.

Figure 10 (a) Acceleration signals with noise at point 1 (b) Fourier spectrum of acceleration with noise at point 1

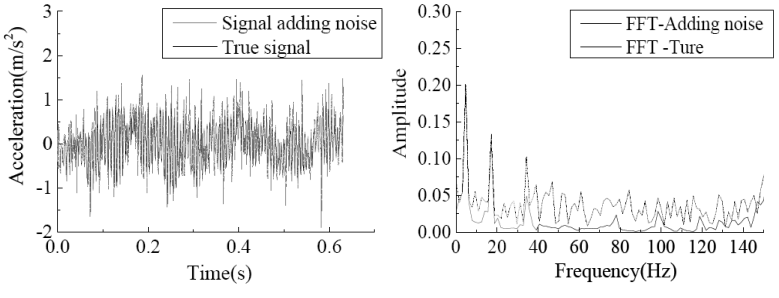

(a) (b)

Figure 11 (a) Denoised acceleration signals at point 1 (b) Fourier spectrum of denoised acceleration at point 1

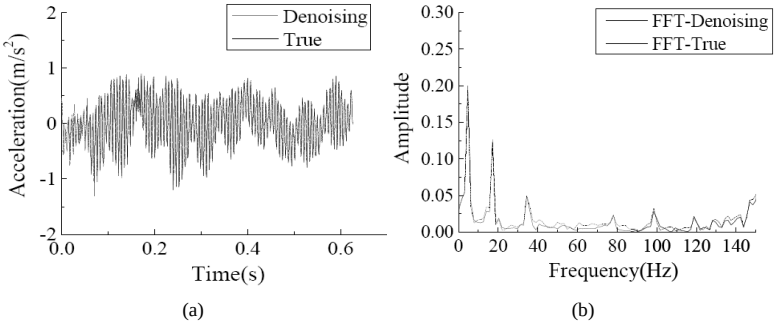

(a) (b)

The vibration displacement was calculated by integrating the acceleration twice in the frequency domain, which can ensure the reliability of the signal and achieve a high precision. There are two equilibrium conditions to meet the application: the velocity and displacement at the measuring points should be idealised as zero before the moving loads enter into the beam, and the beam vibration will be decay to the initial equilibrium state after the moving loads leave the beam. The two conditions can be used to eliminate the trend term in the integration process; thus, the vibration displacement is calculated as shown in Figure 12(a).

Figure 12 (a) Calculated vibration displacement signal at point 2 (b) reconstructed dynamic displacement signal at point 2

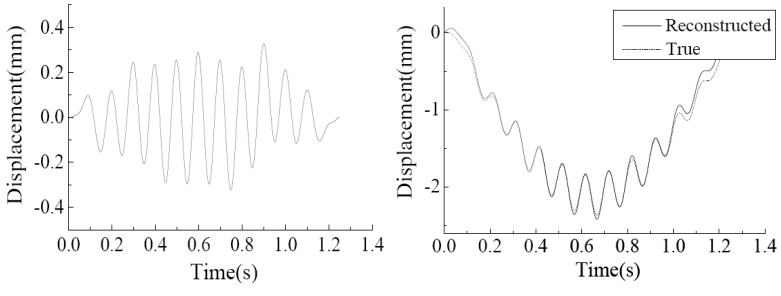

The reconstructed displacement signal shown in Figure 12(b) generally matched the true signal with a relative error of 2.5%, and deviations occurred mainly in the higher frequency range and at both ends of the beam. The deviations were caused by error accumulation in the integration process as well as the end effects, which refers to the divergence phenomenon in the signal decomposition, occurring during the EMD decomposition. When the deviation or uncertainty occurred in the calculation of maximum or minimum values of the signal, errors may arise in the calculated envelope curve and further lead to a divergence of the EMD results.

6.3 Moving load identification

The modal displacement can be obtained using the reconstructed displacement signal through equation (2), and the modal velocity and acceleration can be obtained via numerical differentiation. By substituting the modal displacement, velocity and acceleration into equation (3), the value of the moving load can be identified by the IMII method, while the measurements in time domain can be directly applied to TDM algorithm. Three cases, in which the load moved on the beam at speeds of 10, 20, and 30 m/s, were considered for load identification of the front and rear axles, and the identified results are shown in Figure 13. In the figure, 'true' is the load identified by the TDM from the true dynamic displacement generated by the FE simulation, and 'Recon1' and 'Recon2' are the results identified by the IMII and TDM method based on the reconstructed displacement from polluted strain and acceleration responses, respectively.

The time-varying loads can be identified by the IMII and TDM method when moving across the bridge and the results certify a high reliability for load identification from the reconstructed displacement, by which the noise corruption problem is overcome and the identification error is constrained within a reasonable range of 6%.

Figure 13 Identified results for the time-variable moving load, (a) front-axle at v_1 = 10 m/s (b) rear-axle at v_1 = 10 m/s (c) front-axle at v_1 = 20 m/s (d) rear-axle at v_1 = 20 m/s (e) front-axle at v_1 = 30 m/s (f) rear-axle at v_1 = 30 m/s

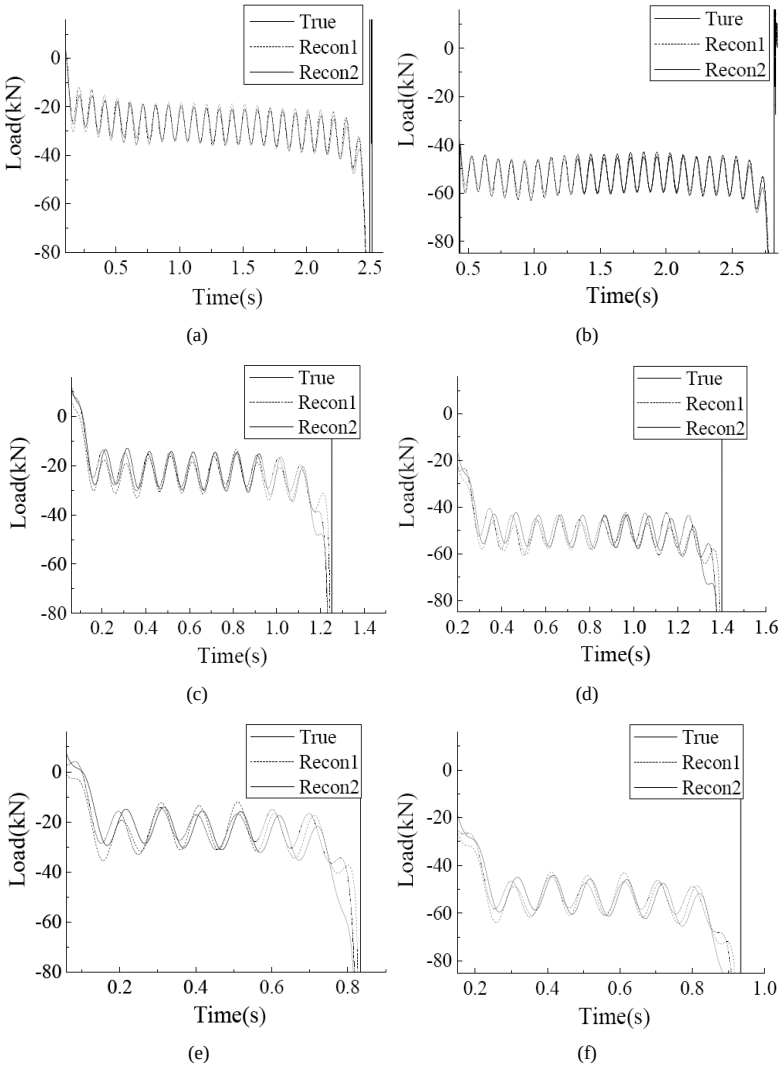

7 Laboratory experiment validation

7.1 Experiment introduction

A simply supported RC slab was constructed for the experiment to validate the proposed theory in application. The length of the slab was 3.6 m, and the width was 0.4 m with a thickness 0.055 m. The cross-section and reinforcement layout of the test specimen are shown in Figure 14(a). Two leading beams with a length of 0.5 m at both ends, which were utilised as the speed guiding way for the model car getting on and off the slab, are shown in Figure 14(b).

Figure 14 (a) Reinforcement layout of the cross-section (b) Structural dimensions and instrumentation layout (see online version for colours)

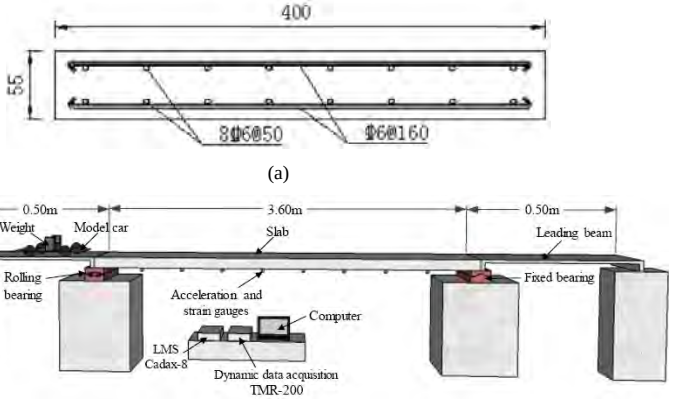

7.2 Structural dynamic test

Before the moving load identification, a multi-reference impact test (MRIT) was conducted to obtain the modal parameters. Due to the limitations of equipment channels, the measurement points were divided into four testing cases by arranging four reference points, as shown in Figure 15. LMS Cadax-8 data acquisition was used to acquire the hammer impact force and acceleration signals. A sampling frequency of 2,048 Hz was selected to capture the impact force at high resolution in the time domain. Each point was hammered three times, and the complex mode indicator function (CMIF) was utilised in the modal analysis. The singular value curves of the frequency response functions (FRFs) produced by the CMIF method are shown in Figure 16, including four curves for each of the reference points.

The FE model was established through Midas software to obtain analytical modal information, which was used to compare with the modal analysis results obtained by the CMIF method in Table 1. The measured and calculated dynamic characteristics are

similar; thus, the FE simulating structure is capable of reflecting the performance of the actual structure.

Figure 15 Instrumentation layout of the modal test

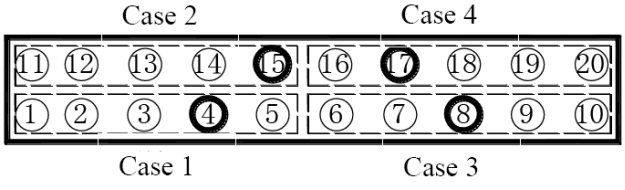

Figure 16 Mode extraction by the CMIF method (see online version for colours)

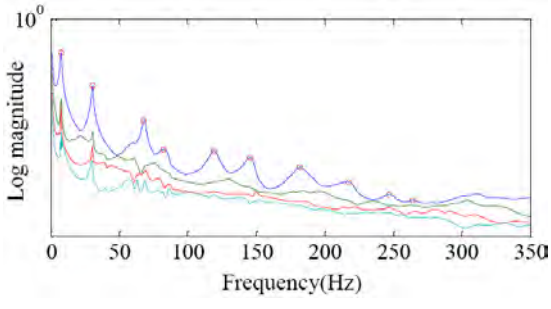

Table 1 Dynamic test results obtained by the MRIT (see online version for colours)

Mode	*FEM simulation*		*CMIF measurement*	
	Frequency (Hz)	*Mode shape*	*Frequency (Hz)*	*Mode shape*
1	7.49		7.50	
2	29.98		30.25	
3	67.33		67.75	
4	81.53		82.01	
5	119.62		118.75	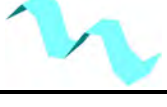

7.3 Moving load experiment

The top of the leading beam was connected to the slab top, and the edge of the beam was very close to the edge of the slab without direct contact. The acceleration and dynamic strain were measured in the experiment, and 8 measurement points were setup on the structure along the longitudinal direction, as shown in Figure 17(a). According to the vehicle speed and loaded mass, 12 cases were scheduled in the experiment, as shown in Table 2. The cases included three sets of vehicle speeds, i.e., v_1 = 0.12 m/s, v_2 = 0.24 m/s, and v_3 = 0.32 m/s, and four sets of vehicle loaded masses, i.e., m_1 = 5 kg, m_2 = 10 kg, m_3 = 15 kg, and m_4 = 20 kg. To verify the monitored dynamic displacement at point 4, a high-speed camera (SONY FDR-AX700) was used to accurately measure the dynamic displacement. The flexural stiffness of the bridge model is estimated to be 188.28 kN/m^2 by loading weights and monitoring the deflection.

Table 2 Load cases of the moving load experiment

Case	*Speed/(m/s)*	*Mass/(kg)*	*Case*	*Speed/(m/s)*	*Mass/(kg)*
1	0.12	5	7	0.12	15
2	0.24	5	8	0.24	15
3	0.32	5	9	0.32	15
4	0.12	10	10	0.12	20
5	0.24	10	11	0.24	20
6	0.32	10	12	0.32	20

Figure 17 (a) Instrumentation layout for data acquisition (b) Picture of the instrumentation (c) Moving load vehicle and target displacement (see online version for colours)

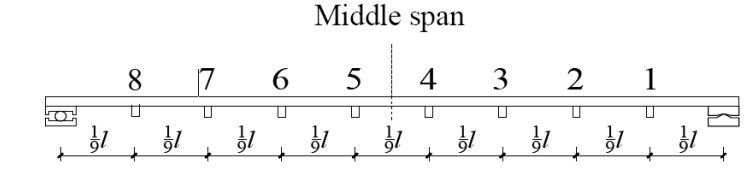

(a)

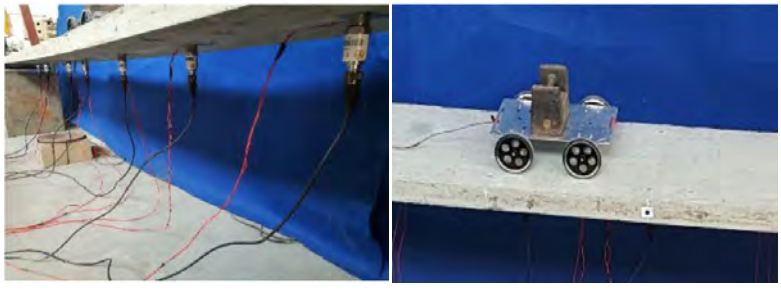

(b) (c)

7.4 Experiment results

According to the dynamic strain signals measured when the vehicle is travelling on the bridge, the raw signal contained a large amount of noise interference, and the high-frequency part was mainly composed of the vibration strains induced by the noise and inertial force. The static strain in the low-frequency domain and the dynamic strain in the high-frequency domain can be separated through EMD. For example, the decomposed results at instrumentation point #4 in case 4 is shown in Figure 18, in which the decomposed signal becomes smooth and the strain reaches the peak when the load passes the instrumentation point. The static strain obtained by the EMD method was used to derive the displacement responses caused by the static loads. After using the data acquired from eight strain sensors and calculating the curvature function by the iterative algorithm, the static displacement under the moving loads could be identified as shown in Figure 19.

Figure 18 EMD of the strain signal at point #4 in case 4, (a) IMF signals (b) static strain

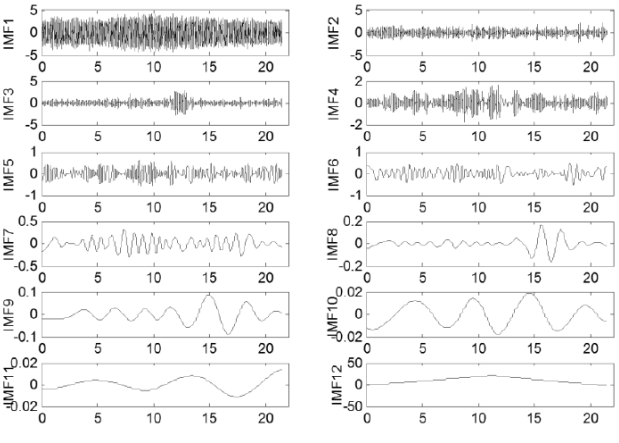

(a)

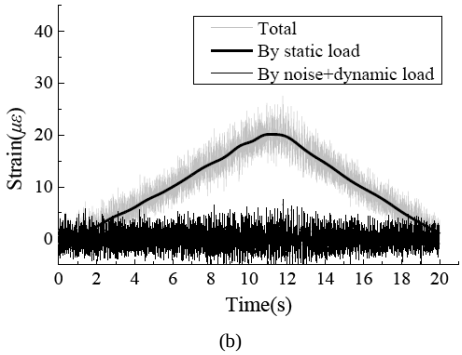

(b)

Figure 19 Identified static displacement results in case 4

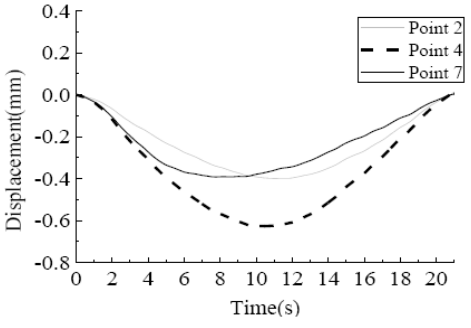

Figure 20 (a) Calculated vibration displacement at point #4 in case 4 (b) Different reconstructed displacements at different points in case 4

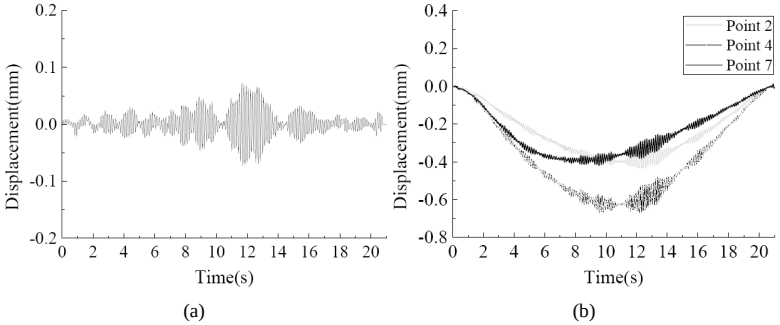

(a) (b)

The identified vibration displacement was calculated from the acceleration signal according to the integration flowchart in Figure 5. Noise reduction was performed on the acquired signal using the LMS algorithm, in which the filter order was set as 100 and the step factor was set as 0.005. Then, the velocity and displacement were obtained by integrating the signal in the frequency domain via MATLAB. The calculated vibration displacement in case 4 is shown in Figure 20. By comparing the results in various cases, the model car moving at a low speed resulted in more obvious high-frequency vibrations of the displacement due to a longer duration on the bridge model than the high-speed model car. The reconstructed displacements obtained by combining the static displacement and vibration displacement are shown in Figure 20(b).

A comparison between the reconstructed displacements and the displacements measured via a high-speed camera at point #4 is illustrated in Figure 21. The measured displacement and reconstructed displacement at point #4 fit well, and the errors at the peak values are less than 3% when the loads moving across the measuring point. The comparison results show that the vibration displacement was accurately restored by the integration of the acceleration signal in the frequency domain. The deflection matched the actual deformation, which indicated that it is capable of reaching the requirement of

the high accuracy measurement by using the strain values for structural curvature reconstruction.

Figure 21 Comparison of the displacement at point #4 in case 4

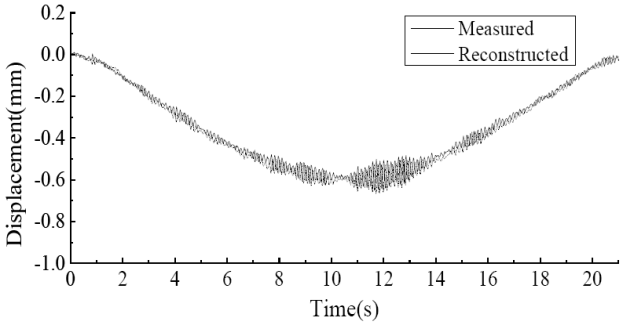

Figure 22 Moving load identification results, (a) case 1 (b) case 4 (c) case 8 (d) case 11

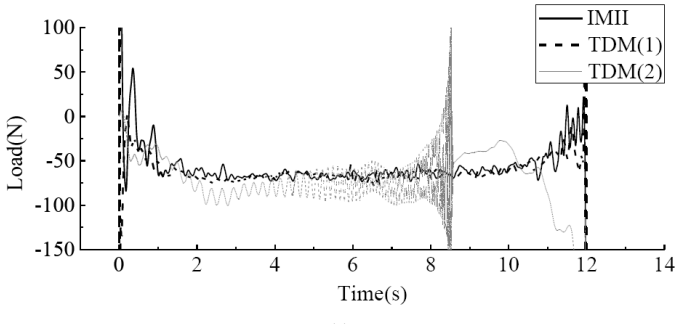

(a)

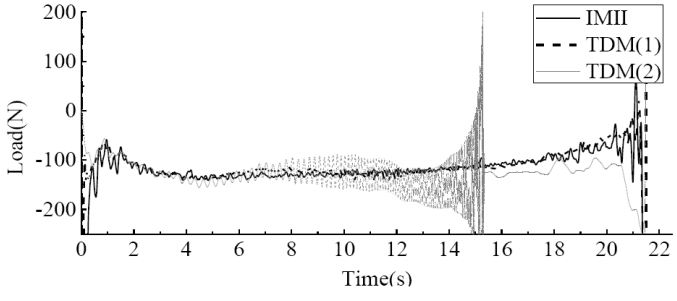

(b)

Figure 22 Moving load identification results, (a) case 1 (b) case 4 (c) case 8 (d) case 11 (continued)

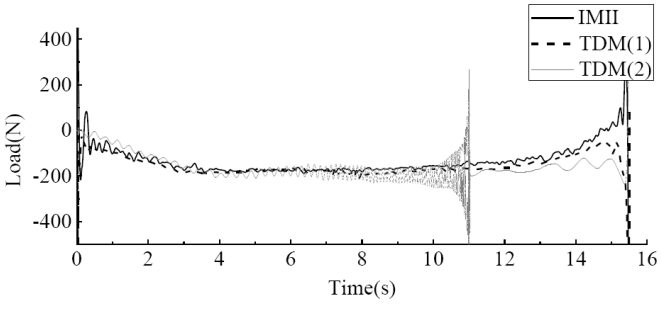

(c)

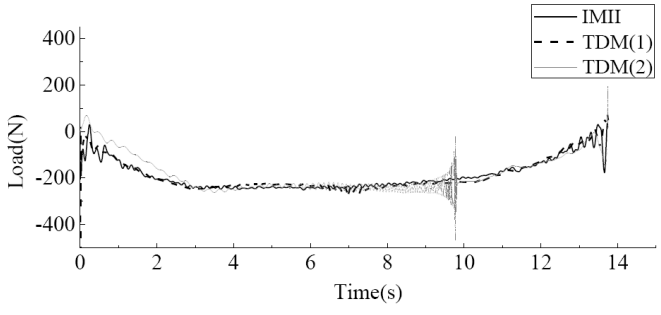

(d)

Load identification was carried out with the reconstructed displacement under various cases, and a small portion of the identified results is shown in Figures 22 and 23, where 'IMII' denotes the results using the IMII method with the reconstructed signals, 'TDM(1)' presents the results using the TDM method with the reconstructed signals, while 'TDM(2)' presents the results using the traditional TDM method without the proposed signal reconstruction and the time-varying loads were identified from the dynamic strains filtered by a low-pass filter. Considering the mass of the entire model car and the loaded weights, the actual loads under cases 1, 4, 8 and 11 are identified as 72.8 N, 122.8 N, 172.8 N and 222.8 N, respectively, which are consistent with the true values. The reconstructed displacement illustrates that the information regarding the single-axle load when moving across the measuring point cannot be adequately identified from the trend of the entire curve. A direct comparison of the identified results illustrates that both the IMII method and TDM are capable of estimating the moving axle loads accurately under different vehicle speed and mass cases after signal processing and optimisation proposed by the author, while the results by the traditional method, employing a low-pass filter for noise reduction, exhibits relatively large fluctuations and critical ill-posedness. Furthermore, the IMII computation required less time than the TDM and was more sensitive to interference noise.

Figure 23 Histogram of the moving load identification, (a) IMII method in case 1 (b) TDM in case 1 (c) IMII method in case 4 (d) TDM in case 4 (e) IMII method in case 8 (f) TDM in case 8 (g) IMII method in case 11 (h) TDM in case 11

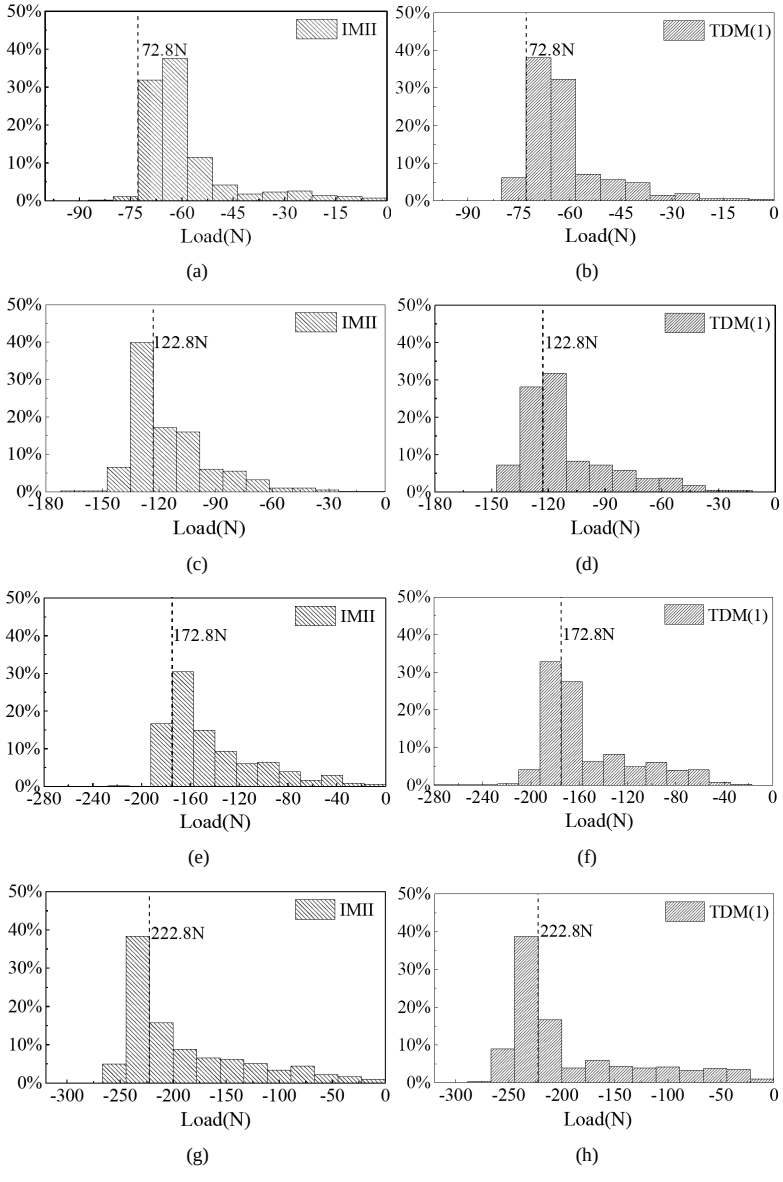

8 Conclusions

Moving load identification aims to resolve the inverse problems that occur when estimating wheel loads in motion from bridge responses. In this paper, a methodology was proposed to reduce the ill-conditioned problem and improve the accuracy of the identification by reconstructing the dynamic displacement of the bridge. The reconstructed displacement is a superposition of the static displacement acquired from the decomposed strain signal and the vibration displacement calculated by denoising the acceleration signal. The following conclusions can be drawn:

1 By employing the measurements from the acceleration and strain sensors, the static and vibration displacements can be calculated to reconstruct the dynamic displacements for further moving load identification of the bridge. As indicated from the load identification results of the FE analysis and laboratory experiment, the reconstructed displacement signal can accurately identify the moving loads under different testing cases, which is effective for overcoming the ill-conditioned problem and achieving a high level of accuracy.

2 The adaptive LMS algorithm for noise reduction can directly filter the noise through signal processing and improve the signal-to-noise ratio. However, the efficiency of noise reduction and the computation rate may be influenced by the convergence ratio.

3 Since the low-frequency noise causes greater corruption on the observed acceleration signal during integration, integration of the denoised signal in the frequency domain can achieve better restoration of the vibration displacement than that in the time domain. Moreover, the trend generated in the integration can be eliminated by simulating it with the least squares method.

Acknowledgements

The authors sincerely appreciate the funding support provided by the National Key Research and Development Program of China (Nos. 2016YFC0701400, 2016YFC0701308), the National Natural Science Foundation of China (NSFC) (Nos. 51878264, 51778222), the Key Research and Development Program of Hunan Province (No. 2017SK2220), and the Research and Development Program of Changsha City (No. kq1801010).

References

Asnachinda, P., Pinkaew, T. and Laman, J.A. (2008) 'Multiple vehicle axle load identification from continuous bridge bending moment response', *Engineering Structures*, Vol. 30, No. 10, pp.2800–2817.

Beizma, M.V. and Schanack, F. (2007) 'Collapse of steel bridges', *Journal of Performance of Constructed Facilities*, Vol. 21, No. 5, pp.398–405.

Chan, T.H.T. and Ashebo, D.B. (2006) 'Theoretical study of moving force identification on continuous bridges', *Journal of Sound and Vibration*, Vol. 295, Nos. 3–5, pp.870–883.

Chan, T.H.T. and Yung, T.H. (2000) 'A theoretical study of force identification using prestressed concrete bridges', *Engineering Structures*, Vol. 22, No. 11, pp.1529–1537.

Chan, T.H.T., Ashebo, D.B. and Demeke, B. (2006) 'Moving axle load from multi-span continuous bridge: laboratory study', *Journal of Vibration & Acoustics*, Vol. 128, No. 4, pp.521–526.

Chan, T.H.T., Law, S.S. and Yuan, T.H. (1999) 'An interpretive method for moving force identification', *Journal of Sound and Vibration*, Vol. 219, No. 3, pp.503–524.

Chan, T.H.T., Yu, L. and Law, S.S. (2000) 'Comparative studies on moving force identification from bridge strains in laboratory', *Journal of Sound and Vibration*, Vol. 235, No. 1, pp.87–104.

Chan, T.H.T., Yu, L., Law, S.S. and Yung, T.H. (2001a) 'Moving force identification studies, I: theory', *Journal of Sound and Vibration*, Vol. 247, No. 1, pp.59–76.

Chan, T.H.T., Yu, L., Law, S.S. and Yung, T.H. (2001b) 'Moving force identification studies, II: comparative studies', *Journal of Sound and Vibration*, Vol. 247, No. 1, pp.77–95.

Chen, Z. and Chan, T.H.T. (2017) 'A truncated generalized singular value decomposition algorithm for moving force identification with ill-posed problems', *Journal of Sound and Vibration*, Vol. 401, No. 4, pp.297–310.

Chen, Z., Chan, T.H.T. and Nguyen, A. (2018) 'Moving force identification based on modified preconditioned conjugate gradient method', *Journal of Sound and Vibration*, Vol. 423, No. 9, pp.100–529.

Deng, L. and Cai, C.S. (2010a) 'Bridge model updating using response surface method and genetic algorithm', *Journal of Bridge Engineering*, Vol. 15, No. 5, pp.553–564.

Deng, L. and Cai, C.S. (2010b) 'Identification of dynamic vehicular axle loads: theory and simulations', *Journal of Vibration and Control*, Vol. 16, No. 4, pp.2167–2194.

Deng, L. and Cai, C.S. (2011) 'Identification of dynamic vehicular axle loads: demonstration by a field study', *Journal of Vibration and Control*, Vol. 17, No. 2, pp.183–195.

González, A., Rowley, C. and Obrien, E.J. (2008) 'A general solution to the identification of moving vehicle forces on a bridge', *International Journal for Numerical Methods in Engineering*, Vol. 75, No. 3, pp.335–354.

Huang, N.E. (2000) 'New method for nonlinear and nonstationary time series analysis: empirical mode decomposition and Hilbert spectral analysis', *Proceedings of SPIE – The International Society for Optical Engineering*, Vol. 4056, pp.197–209.

Huang, N.E., Shen, Z., Long, S.R. et al. (1998) 'The empirical mode decomposition and Hilbert spectrum for nonlinear and nonstationary time series analysis', *Proceedings of Royal Society*, London, Vol. 454, pp.903–995.

Kowm, D., Kim, M., Hong, C. and Cho, S. (2014) 'Artificial neural network based short term load forecasting', *International Journal of Smart Home*, Vol. 8, No. 3, pp.145–150.

Law, S.S. and Fang, Y. (2001) 'Moving force identification: optimal state estimation approach', *Journal of Sound and Vibration*, Vol. 239, No. 2, pp.233–254.

Law, S.S. and Lu, Z.R. (2005) 'Time domain response of a prestressed beam and prestress identification', *Journal of Sound and Vibration*, Vol. 288, Nos. 1–2, pp.1011–1025.

Law, S.S. and Zhu, X.Q. (2000) 'Study on different beam models in moving force identification', *Journal of Sound and Vibration*, Vol. 234, No. 4, pp.661–679.

Law, S.S., Bu, J.Q., Zhu, X.Q. and Chan, S.L. (2004) 'Vehicle axle loads identification using finite element method', *Engineering Structures*, Vol. 26, No. 8, pp.1143–1153.

Law, S.S., Bu, J.Q., Zhu, X.Q. and Chan, S.L. (2007) 'Moving load identification on a simply supported orthotropic plate', *International Journal of Mechanical Sciences*, Vol. 49, No. 11, pp.1262–1275.

Law, S.S., Chan, T.H.T. and Zeng, Q.H. (1997) 'Moving force identification: a time domain method', *Journal of Sound and Vibration*, Vol. 201, No. 1, pp.1–22.

Law, S.S., Chan, T.H.T. and Zeng, Q.H. (1999) 'Moving force identification: a frequency and time domains analysis', *Journal of Dynamic Systems, Measurement, and Control*, Vol. 121, No. 3, pp.394–401.

Law, S.S., Chan, T.H.T., Zhu, Q.X. and Zeng, Q.H. (2001) 'Regularization in moving force identification', *Journal of Engineering Mechanics*, Vol. 127, No. 2, pp.136–148.

Lu, C.N., Wu, H.T. and Vemuri, S. (1993) 'Neural network based short term load forecasting', *IEEE Transactions on Power Systems*, Vol. 8, No. 1, pp.336–342.

Lu, Z.R. and Law, S.S. (2005) 'Identification of prestress force from measured structural responses', *Journal of Mechanical Systems and Signal Processing*, Vol. 20, No. 8, pp.2186–2199.

Lydon, M., Taylor, S.E., Robinson, D., Mufti, A. and O'Brien, E.J. (2016) 'Recent developments in bridge weigh in motion (B-WIM)', *Journal of Civil Structural Health Monitoring*, Vol. 6, No. 1, pp.69–81.

O'Brien, E.J., Žnidarič, A. and Ojio, T. (2008) 'Bridge weigh-in-motion – latest developments and applications worldwide', *International Conference on Heavy Vehicles*, Paris.

O'Connor, C. and Chan, T.H.T. (1988) 'Dynamic wheel loads from bridge strains', *Journal of Structure and Engineering*, Vol. 114, No. 8, pp.1703–1723.

Pan, C.D. and Yu, L. (2014) 'Moving force identification based on firefly algorithm', *Advanced Materials Research*, Vol. 919, No. 1, pp.329–333.

Park, M.S., Jo, B.W., Kim, S. and Lee, J. (2009) 'Vehicle signal analysis using artificial neural networks for a bridge weigh-in-motion system', *Sensors*, Vol. 9, No. 10, pp.7943–7956.

Pinkaew, T. (2006) 'Identification of vehicle axle loads from bridge responses using updated static component technique', *Engineering Structures*, Vol. 28, No. 11, pp.1599–1608.

Pinkaew, T. and Asnachinda, P. (2007) 'Experimental study on the identification of dynamic axle loads of moving vehicles from the bending moments of bridges', *Engineering Structures*, Vol. 29, No. 9, pp.2282–2293.

Sanchez, J. and Benaroya, H. (2014) 'Review of force reconstruction techniques', *Journal of Sound and Vibration*, Vol. 333, No. 14, pp.2999–3018.

Wang, W., Deng, L. and Shao, X. (2016) 'Fatigue design of steel bridges considering the effect of dynamic vehicle loading and overloaded trucks', *Journal of Bridge Engineering*, Vol. 21, No. 9, p.4016048.

Yu, L. and Chan, T.H.T. (2002) 'Moving force identification from bending moment responses of bridge', *Structural Engineering and Mechanics*, Vol. 14, No. 2, pp.151–170.

Yu, L. and Chan, T.H.T. (2003) 'Moving force identification based on the frequency-time domain method bending moment responses of bridge', *Journal of Sound and Vibration*, Vol. 261, No. 2, pp.329–349.

Yu, L. and Chan, T.H.T. (2007) 'Recent research on identification of moving loads on bridges', *Journal of Sound and Vibration*, Vol. 305, Nos. 1–2, pp.3–21.

Yu, Y., Cai, C.S. and Deng, L. (2016) 'State-of-the-art review on bridge weigh-in-motion technology', *Journal of Advances in Structural Engineering*, Vol. 19, No. 9, pp.1514–1530.

Zhu, X.Q. and Law, S.S. (1999) 'Moving force identification on a multi-span continuous bridge', *Journal of Sound and Vibration*, Vol. 228, No. 2, pp.377–396.

Zhu, X.Q. and Law, S.S. (2001a) 'Identification of moving loads on an orthotropic plate', *Journal of Vibration and Acoustics*, Vol. 123, No. 2, pp.238–244.

Zhu, X.Q. and Law, S.S. (2001b) 'Orthogonal function in moving loads identification on a multi-span bridge', *Journal of Sound and Vibration*, Vol. 245, No. 2, pp.329–345.

Zhu, X.Q. and Law, S.S. (2002a) 'Moving load identification through regularization', *Journal of Engineering Mechanics*, Vol. 128, No. 9, pp.989–1000.

Zhu, X.Q. and Law, S.S. (2002b) 'Practical aspects in moving load identification', *Journal of Sound and Vibration*, Vol. 258, No. 1, pp.123–146.

Zhu, X.Q. and Law, S.S. (2003a) 'Dynamic axle and wheel loads identification: laboratorary studies', *Journal of Sound and Vibration*, Vol. 268, No. 5, pp.855–879.

Zhu, X.Q. and Law, S.S. (2003b) 'Identification of moving interaction forces with incomplete velocity information', *Mechanical Systems & Signal Processing*, Vol. 17, No. 6, pp.1349–1366.

Zhu, X.Q. and Law, S.S. (2003c) 'Time domain identification of moving loads on bridge deck', *Journal of Vibration and Acoustics*, Vol. 125, No. 2, pp.187–198.

Zhu, X.Q. and Law, S.S. (2006) 'Moving load identification on multi-span continuous bridges with elastic bearings', *Journal of Mechanical Systems and Signal Processing*, Vol. 20, No. 7, pp.1759–1782.

Zhu, Z., Gao, X. and Cao, L. (2016) 'Analysis on the adaptive filter based on LMS algorithm', *Journal of Optik*, Vol. 127, No. 11, pp.4698–4704.